Revealing Seasonal Plasticity of Whole-Plant Hydraulic Properties Using Sap-Flow and Stem Water-Potential Monitoring

Zhechen Zhang[1], Huade Guan[1*], Erik Veneklaas[2], Kamini Singha[3], and Okke Batelaan[1]

[1]National Centre for Groundwater Research and Training, College of Science & Engineering, Flinders University, Adelaide, South Australia, Australia.
[2]School of Biological Sciences, The University of Western Australia, Perth, Western Australia, Australia
[3]Department of Geology & Geological Engineering, Hydrologic Science and Engineering Program, Colorado School of Mines, Golden, CO, USA.

Corresponding author: Huade Guan (huade.guan@flinders.edu.au)

Abstract. Plant hydraulic properties are critical to predicting vegetation water use as part of land-atmosphere interactions and plant responses to drought. However, current measurements of plant hydraulic properties are labour-intensive, destructive, and difficult to scale up, consequently limiting the comprehensive characterization of whole-plant hydraulic properties and hydraulic parameterization in land-surface modelling. To address these challenges, we develop a pumping-test analogue method, using sap-flow and stem water-potential data to derive whole-plant hydraulic properties, namely maximum hydraulic conductance, effective capacitance, and Ψ_{50} (water potential at which 50% loss of hydraulic conductivity occurs). Experimental trials on *Allocasuarina verticillata* indicate that the parameters derived over short periods (around 7 days) exhibit good representativity for predicting plant water use over at least one month. We applied this method to estimate near-continuous whole-plant hydraulic properties over one year, demonstrating its potential to supplement existing labour-intensive measurement approaches. The results reveal the seasonal plasticity of the effective plant hydraulic capacitance. They also confirm the seasonal plasticity of maximum hydraulic conductance and the hydraulic vulnerability curve, known in the plant physiology community while neglected in the hydrology and land-surface modelling community. It is found that the seasonal plasticity of hydraulic conductance is associated with climate variables, providing a way forward to represent seasonal plasticity in models. The relationship between derived maximum hydraulic conductance and Ψ_{50} also suggests a trade-off between hydraulic efficiency and safety of the plant. Overall, the pumping-test analogue offers potential for better representation of plant hydraulics in hydrological modelling, benefitting land-management and land-surface process forecasting.

1 Introduction

Plant hydraulic properties, such as maximum xylem hydraulic conductance, vulnerability to cavitation, and maximum stomatal conductance, are fundamental plant functional traits regulating hydraulic processes in plants. They play critical roles in regulating transpiration and growth by controlling plant water uptake (Anderegg and Meinzer, 2015; Matheny et al., 2017a), and are instrumental in predicting plant water storage (Huang et al., 2017), and drought-driven tree mortality risk (Liu et al., 2017; Powell et al., 2017; Torres-Ruiz et al., 2024). Hydraulic properties of different species and plant communities reflect different water-use strategies, which determine various responses to root-zone moisture conditions (Matheny et al., 2017b; Barros et al., 2019). Consequently, plant hydraulic properties are critical to predicting plant water use as part of land-atmosphere interactions and ecosystem responses to drought.

Plant hydraulic properties exhibit temporal variability. Variations can be expected across ontogeny (Mencuccini, 2002), between seasons (Jacobsen et al., 2007), and in response to hydroclimatic events such as droughts (Anderegg and Callaway, 2012). For example, the maximum hydraulic conductance can change due to carbon allocation to stem growth (Buckley and Roberts, 2006; Potkay et al., 2021). Some plant physiology studies have demonstrated that plant hydraulic properties have seasonal plasticity, which means they are time-variant in the

year. Past studies have reported that the maximum hydraulic conductance and the Ψ_{50} (xylem water potential at which 50% loss of hydraulic conductivity occurs) values of several tree species vary significantly in different seasons (e.g., *Artemisia tridentata* (Kolb and Sperry, 1999), several Californian species (Jacobsen et al., 2007), several Mediterranean species (Sorek et al., 2022), and *Pinus halepensis* (Feng et al., 2023)). Similarly, Li et al. (2023) reported that most of the leaf hydraulic traits of Korean pine and spruce significantly changed over four months. Ecological modelers found that the hydraulic properties calibrated in one season are not transferable to other seasons (Steppe et al., 2008; Baert et al., 2014; Salomón et al., 2017), which is likely due to the plasticity of plant hydraulic properties. Despite the evidence of seasonal plasticity of hydraulic properties, it is not known yet how common this phenomenon is and what mechanisms drive it (Feng et al., 2023), in part become of limited high-frequency measurements across seasons. Although continuous monitoring of plant water use has become more common, very few studies have combined sap flux and water status measurements, which may be key to informing the seasonal variation in plant hydraulics.

Despite evidence of seasonal plasticity in plant hydraulic properties, they are largely treated as constant parameters in both single-plant models (Bohrer et al., 2005; Christoffersen et al., 2016; Deng et al., 2017) and ecosystem-scale models (Kennedy et al., 2019; Li et al., 2021), due to the complexity of parameterizing time-variant properties. There have been a few attempts to consider plant hydraulics in land-surface models (Kennedy et al., 2019; Li et al., 2021; Xie et al., 2023; Paschalis et al., 2024); although these efforts have significantly improved model performance, none of the models utilize time-variant hydraulic properties. To facilitate time-invariant parameterization, some models have simplified the structure of their hydraulic module; for example, the latest Noah-MP-PHS model includes only hydraulic conductance and excludes hydraulic capacitance (Li et al., 2021). The work of Jiménez-Rodríguez et al. (2024) suggests that parameterization of maximum hydraulic conductance is an important yet unresolved issue in land-surface models such as CLM. While time-invariant parameterization of plant hydraulics in models is challenging, time-variant parameterization is even more difficult.

Current methods for estimating plant hydraulic properties are one limitation on parameterization of plant hydraulics in models. The most commonly used measurements of hydraulic properties involve collecting 'snapshots' in time (for example, dehydration methods to measure hydraulic conductivity) (Sperry et al., 1988; Zhang et al., 2018). These ‘snapshot’ methods are typically conducted in the laboratory using stem sections collected from the field. They are destructive and labor-intensive, resulting in static and limited data (Novick et al., 2022) that cannot capture seasonal variation. Furthermore, hydraulic properties measured at stem scales are difficult to scale up to representative whole-plant parameter values required for modeling. Few studies have investigated whole-plant hydraulic properties based on field measurements (Zeppel et al., 2008; Deng et al., 2017), and such early attempts still adopted time-invariant hydraulic vulnerability curves. Due to data limitations, applying hydraulic properties of specific species in a land-surface model is quite challenging. Most studies use plant hydraulic properties based on the Plant Functional Type (PFT) classification network (Paschalis et al., 2024; Raghav et al., 2024). Including different species within the same PFT classification neglects inter- and intra-species variation in hydraulic properties. The static and limited plant hydraulic properties from current lab-based methods hinder the ability to capture temporal dynamics, whole-plant representation, and intra- and inter-species variability.

Model-data fusion methods have recently shown potential to address challenges such as inter- and intra-species variability and whole-plant representativeness (Liu et al., 2020b; Lu et al., 2022; Loritz et al., 2022), but they still cannot capture the temporal variability of hydraulic properties. Such approaches, combined with a given model, estimate the properties that best match the observed temporal variation of evapotranspiration or sap flow. Liu et al. (2021) derived ecosystem-scale plant traits (stomatal conductance and Ψ_{50}) across the globe using a model-data fusion approach constrained by remote-sensing products of evapotranspiration, vegetation optical depth, and soil moisture. Building upon this foundation, Lu et al. (2022) estimated species-specific hydraulic properties based on sap flow measurements. Although these model-data fusion methods have shown promise in enhancing our understanding of spatial and intra- and inter-species variations of hydraulic properties, at the whole-plant scale, quantifying temporal variation of plant hydraulics remains a challenge because of the extensive data inputs needed for model-data fusion methods.

This paper aims to develop a new method to estimate plant hydraulic properties based on continuous and non-destructive field monitoring. Specifically, we quantify whole-plant hydraulic conductance and capacitance using sap-flow and stem water-potential data. We test this new method on several drooping sheoak trees and investigate the seasonal variation in hydraulic properties of this species.

2 Methodology

2.1 Pumping-test analogue theory development

We develop a pumping-test analogue to estimate time-variant plant hydraulic properties, borrowing from the concept of pumping tests in hydrogeology where the hydraulic properties of an aquifer are estimated based on hydraulic head responses (measured at observation wells) to the disburbance induced at the pumping well. In the soil-plant continuum, root water uptake and transpiration introduce the hydraulic disturbance, resulting in simultaneous plant water-potential responses. Therefore, by measuring the "pumping" — dynamic transpiration (or sap flow) and the "corresponding response", i.e., the plant water-potential change, and relating these two aspects through a physically based model, we can derive the key hydraulic properties that govern plant hydraulic processes, such as plant hydraulic conductance and capacitance. In addition, plants also work as hydraulic 'capacitors' that temporally store and release water depending on the water demand from the canopy and water uptake from the root zone, resulting in diel fluctuation of plant water potential. With an increasing number of long-term observations of sap flow and an increasing ability to measure plant water potential in recent years (Restrepo-Acevedo et al., 2024), the approach proposed here is increasingly feasible, providing the necessary data to link water-flux changes with plant water potential and derive key hydraulic properties.

Here, we use a whole-plant hydraulics model to connect measured water flux and water-potential changes. An analogue resistance-capacitance model (RC model) is commonly used to simulate hydraulic processes in the soil-plant-atmosphere continuum, with two parts: plant water-uptake flux and storage change flux. There are a number of RC models of different complexity (Loustau et al., 1998; Cowan, 1965; Steppe et al., 2006; Salomón et al., 2017). The whole-plant RC model (Liu et al., 2021) has the simplest structure with only one circuit (conceptualized model shown in Fig. 1), as follows:

$$E_C = Q - \frac{dS_P}{dt} \quad (1)$$

where E_C (cm^3 cm^{-2} h^{-1}) is transpiration flux density, Q (cm^3 cm^{-2} h^{-1}) is plant water-uptake flux density and $\frac{dS_P}{dt}$ (cm^3 cm^{-2} h^{-1}) is the whole-plant-equivalent transpirable-storage change rate. All flux densities are normalized over the sapwood area. Plant water uptake flux density Q is calculated by a Darcy's law equivalent formulation between two effective nodes, the plant and root-zone nodes (Steppe et al., 2006):

$$Q = k_P * (\psi_{rz} - \psi_P) \tag{2}$$

where k_P (cm^3 cm^{-2} h^{-1} MPa^{-1}) is the whole-plant equivalent hydraulic conductance (defined as the ratio of hydraulic conductivity over the equivalent hydraulic path distance between two points where the two water potentials are specified, ψ_P (MPa) is the effective plant water potential to represent the water status of the plant node, and ψ_{rz} (MPa) is the bulk root-zone water potential.

The hydraulic capacitance C_P (cm^3 cm^{-2} MPa^{-1}) is defined as the ratio of the change in the amount of water storage to the change in water potential (Steppe et al., 2006; Salomón et al., 2017; Hunt et al., 1991):

$$C_P = \frac{dS_P}{d\psi_{P_S}} \tag{3}$$

where ψ_{P_S} (MPa) is the effective water potential at which stored water is held by the plant. Substituting Eq. 2 and Eq. 3 into Eq. 1, the transpiration flux density Ec can be calculated as:

$$E_C = k_P * (\psi_{rz} - \psi_P) - C_P * \frac{d\psi_{P_S}}{dt} \tag{4}$$

The whole-plant conductance varies with effective whole-plant water potential, following a Weibull shape vulnerability curve (Sperry et al., 1998;Ogle et al.,2009; Deng et al., 2017):

$$k_P = k_{max} e^{-\left(-\frac{\psi_P}{d}\right)^c} \tag{5}$$

where k_{max} (cm^3 cm^{-2} h^{-1} MPa^{-1}) is the maximum hydraulic conductance, and d and c are two curve-fitting parameters.

Plant hydraulic conductivity is not only affected by water potential (Eq.5) but also by temperature (Yang et al., 2020; Cochard et al., 2000). Hydraulic conductivity is proportional to the permeability of the porous material and inversely proportional to the dynamic viscosity (Marshall et al., 1996). We assume that the permeability in a root-zone and plant continuum is constant over a short time, as it is only related to the medium structure. Dynamic viscosity, meanwhile, is strongly dependent on the temperature and type of fluid (Marshall et al., 1996), so hydraulic conductance at one specific temperature can be expressed as follows:

$$k_{P,T} = k_{P,T_{ref}} * \frac{\eta_{T_{ref}}}{\eta_T} \tag{6}$$

where $k_{P,T}$ and $k_{P,T_{ref}}$ are hydraulic conductance at specific temperature T and at reference temperature T_{ref}, respectively, and η_T and $\eta_{T_{ref}}$ are water dynamic viscosity at specific temperature T and at reference temperature T_{ref}, respectively. We use Eq.6 to adjust the influence of temperature on hydraulic conductance, allowing the derived values to be standardized to a reference temperature (25 °C in this study). All subsequent hydraulic conductance values presented in this paper are reported for 25 °C. The empirical equation used in this study of water viscosity variation with temperature is as follows (Heggen, 1983; Dingman, 2015):

$$\eta_T = 2.0319 * 10^{-4} + 1.5883 * 10^{-3} * exp\left[-\left(\frac{T^{0.9}}{22}\right)\right] \tag{7}$$

where T is in °C.

The whole-plant hydraulic capacitance also varies with water potential. We adopt the following relation:

$$C_P = C_{max}\left(\frac{\psi_0 - \psi_{P_S}}{\psi_0}\right)^{-p} \quad (8)$$

where C_{max} (cm^3 cm^{-2} MPa^{-1}) is the maximum hydraulic capacitance, and ψ_0 (MPa) and p are empirical parameters (Chuang et al., 2006).

Together, Equations 4-8 define the complete whole-plant hydraulic model. There are three state variables (ψ_P, ψ_{P_S}, and ψ_{rz}) and six parameters ($k_{max,25}$, d, c, C_{max}, ψ_0, and p), all of which are being estimated by this method. Although the conceptualized effective plant water potential ψ_P cannot be measured, water potential in a part of the plant, e.g., the stem, can be monitored using stem psychrometers, which covary with whole-plant effective water potential. Therefore, we assume that the effective plant water potential can be approximated by the stem water potential measured at a specific location. Similarly, the assumption that the water potential of plant water storage ψ_{P_S} is equivalent to the observed stem water potential is a reasonable approximation (Liu et al., 2021).

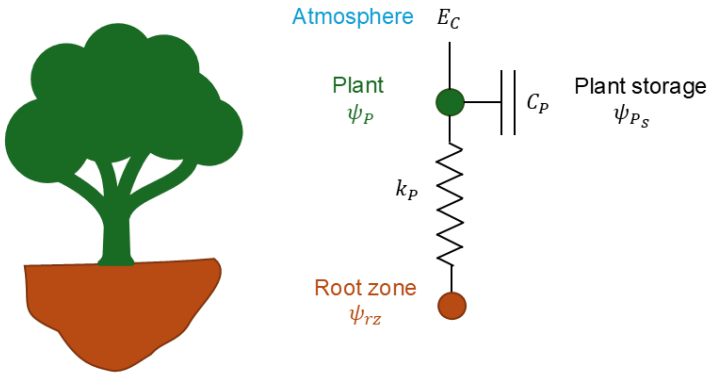

Figure 1: Conceptual diagram of the whole-plant hydraulics model.

2.2 Site and data description

Data collected from three drooping sheoak trees (*Allocasuarina verticillata*) were used in this study to validate the proposed pumping-test analogue method. They grow on a hillslope at the Bedford Park Campus of Flinders University (35°1′49″ S, 138°34′28″ E), Adelaide, South Australia. This site experiences a Mediterranean climate characterized by distinct wet winter and dry summer. Stem water potential was measured by thermocouple psychrometers (PSY1, ICT International Pty Ltd., Australia) at half-hourly intervals. Sap-flow rates were measured at half-hourly intervals at ~1.2 m height of the trunk by heat-pulse sap flow meters (SFM1, ICT International Pty Ltd., Australia). Figure 2 shows the hourly stem water potential and sap-flow rate recordings. Geometric data of the trees and detailed measurement settings were reported in Luo et al. (2020). The tree numbers are the same as in Luo et al. (2020). However, only Trees 2, 3, and 4 are used in this study, as the sap-flow and stem water-potential recordings of Tree 1 were too short for this study. Air temperature and radiation data (in Fig.3a and 3b) were from a weather station located at the Bedford Park Campus. Precipitation data (in Fig.3c) were from a nearby weather station of Kent Town (34.92° S, 138.62°E).

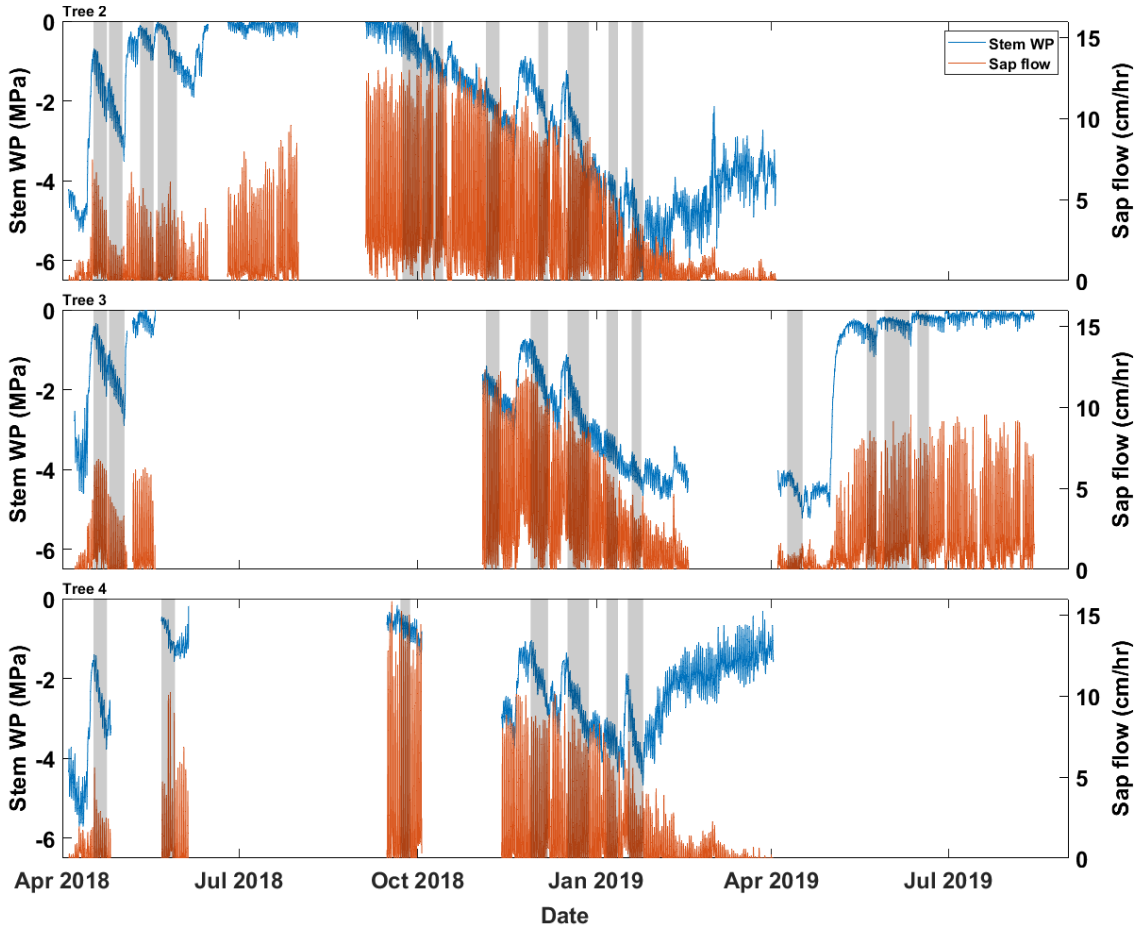

Figure 2: The input data for the pumping-test analogue on three drooping sheoak trees. Blue lines show the hourly stem water-potential recordings and orange lines are the hourly sap-flow rates. The intervals marked in grey are the selected calibration periods for each tree, which are periods without any rainfall.

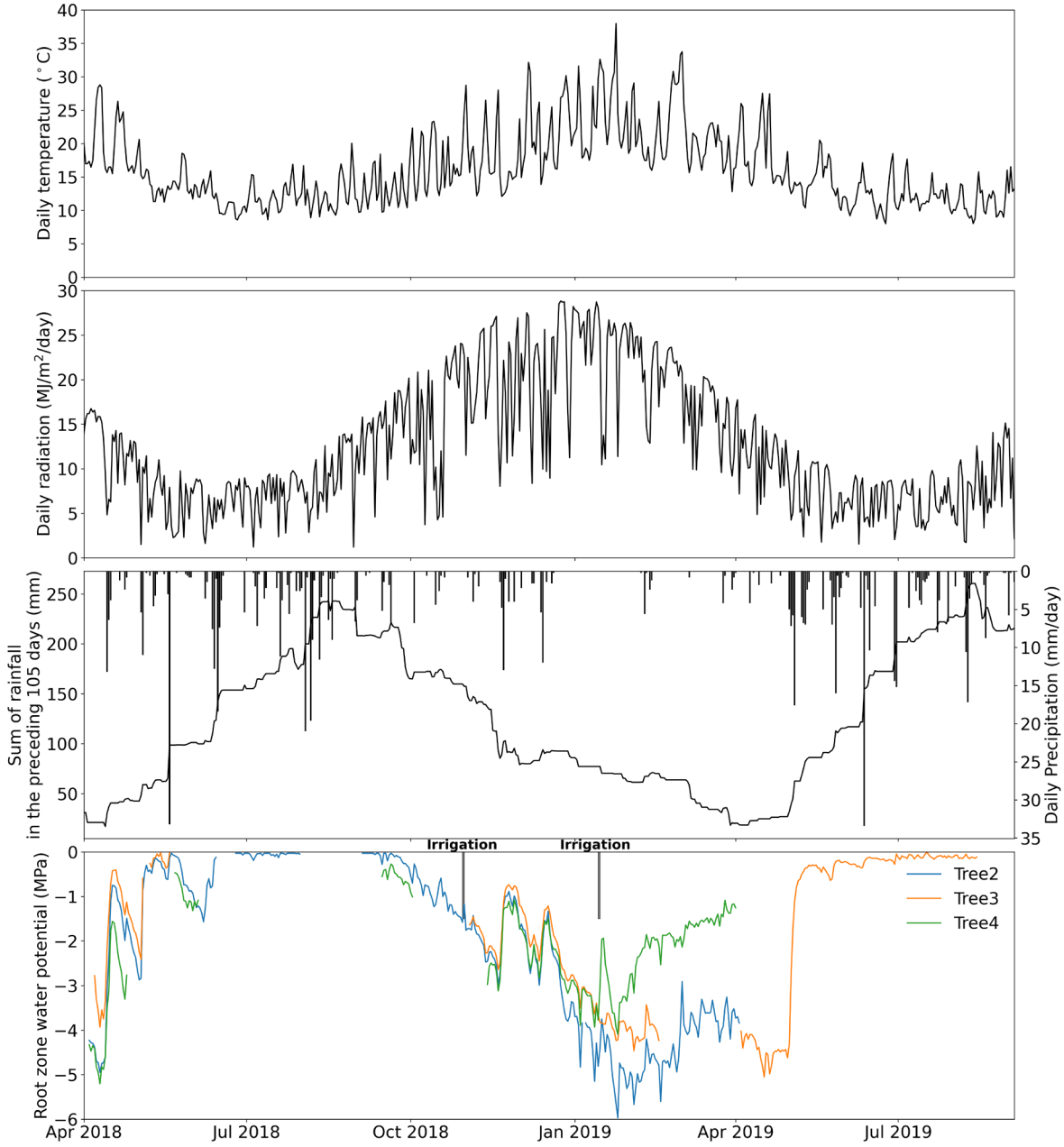

Figure 3: (a) Daily air temperature, (b) radiation, (c) daily precipitation and the sum of rainfall in the preceding 105 days, and (d) the estimated root zone water potential derived from stem water potential of each tree. The irrigation experiments are indicated in panel (d). Two drip irrigation events (not shown in panel (c)) were conducted during the study period. The first occurred on 30 October 2018, applying 80 L of water to Tree 2. The second took place between the late afternoon of 14 January and 15 January 2019, applying 100 L of water to Tree 2 and Tree 4, respectively.

2.3 MCMC Implementation

A Markov Chain Monte Carlo (MCMC) method was used to infer the parameters of the whole-plant hydraulics model because it has been successfully applied for deriving whole-plant hydraulic traits (Liu et al., 2021; Lu et al., 2022), as well as for estimating plant hydraulic model parameters (Deng et al., 2017). We used an MCMC sampling scheme within the DiffeRential Evolution Adaptive Metropolis (DREAM) algorithm (Vrugt et al., 2009). The MCMC chain number was set to 10 and the iteration steps were set to 3000 times per parameter (18000 in total). We took the last 25% of samples as posterior samples, which is a common setting in DREAM applications on hydrological problems (Baig et al., 2022). The objective function we set is the sum of squared

errors (SSE) between the observed and simulated sap flux density (cm/h). The parameters of the whole-plant hydraulic model and their calibration range are shown in Table 1. Since the pumping-test analogue is based on plant hydraulic processes, the hydraulic properties it estimates represent the effective hydraulic properties contributing to transpiration rather than the hydraulic properties measured in the lab. Thus, $k_{max,25}$ and C_{max} correspond to maximum effective hydraulic conductance and capacitance, respectively. All ranges were set as large as reasonable to minimize the chance of missing the global minimum in the optimization. The range of empirical parameters of the capacitance curve was based on the literature (Chuang et al., 2006; Deng et al., 2017; Silva et al., 2022). To minimize the effect of measurement error of stem water potential, we applied a one-hour moving average to the raw measured stem water potential. The predawn bulk root-zone water potential $\psi_{rz,predawn}$ (Fig.3d) was approximated by the measured stem water potential, based on the predawn hydraulic equilibrium assumption (Sperry et al., 2002; Wang et al., 2014; Liu et al., 2020a). Predawn was defined as 3:00 am to 5:00 am in this study, and bulk root-zone water potential ψ_{rz} at other times (Fig.3d) was estimated by interpolation of $\psi_{rz,predawn}$ at either side.

Table 1: Parameters of the whole-plant hydraulic model and calibration range.

Symbol	Description	Range
$k_{max,25}$ (cm/h/MPa)	Maximum effective hydraulic conductance at 25 °C	0-100
c (-)	Conductivity curve-fitting parameter	1.5-5*
d (-)	Conductivity curve-fitting parameter	1.5-5*
C_{max} (cm/MPa)	Maximum effective hydraulic capacitance	0-500
ψ_0 (MPa)	Empirical parameters of capacitance curve	0-5
p (-)	Empirical parameters of capacitance curve	1.5-5

** These fitting parameters are shown in Equation 5. The low boundaries of the conductance-curve fitting parameters were set up as 1.5 to ensure that the conductance curve was S-shaped.*

2.4 Pumping-test analogue validation

First, we validated that the proposed pumping-test analogue framework could derive reasonable hydraulic properties based on sap-flow and stem water-potential data. Given that we interpolated sub-daily bulk root-zone water-potential values between consecutive predawn measurements, precise estimation of bulk root-zone water potentials was hindered in cases of daytime wetting events. To mitigate this issue, we excluded such days and selected periods with at least five days of consecutive predawn stem water-potential reductions as the calibration periods (grey boxes in Fig.2). For example, there were twelve calibration periods for Tree 2 (P1 – P12). The validation periods were not predetermined but rather dynamically extended from each calibration period. This extension proceeded at a rate of one hour per step in both temporal directions until it encompassed the entirety of the dataset. This approach offered a flexible way to assess the representativeness of the properties derived during the calibration period across different times of the year.

We used three criteria to filter the derived hydraulic properties for further seasonal variation analysis. The first criterion was that the Nash-Sutcliffe Efficiency (NSE) must be higher than 0.6 in the calibration period. The second was that the extended validation period with NSE higher than 0.6 must be longer than 20 days. In addition to the calibration and validation criteria, ensuring the convergence of posterior samples was another vital factor to control the reliability and stability of parameter estimation. The third criterion was that the Gelman and Rubin statistics (R_stat) must be lower than 1.2 to confirm the convergence of the MCMC process (Gelman and Rubin, 1992; Deng et al., 2017).

2.5 Deriving near-continuous plant hydraulic properties

After successfully validating that the pumping-test analogue framework could derive representative plant hydraulic properties using short-term data, we applied this method to obtain near-continuous plant hydraulic properties for analysing the relationships between the properties ($k_{max,25}$, Ψ_{50}, and C_{max}) and climate variables. In this study, we selected three key climate variables that are commonly known to influence plants: radiation, temperature, and precipitation. Unlike the validation phase, the actual application did not require selecting no-rain periods as calibration periods. Instead, we used a dynamic-window approach to estimate plant hydraulic properties every day. The influence of rainfall on root-zone water potential remained a concern; therefore, we selected a 20-day duration for the dynamic window. Longer windows can help mitigate the influence of rainfall, because rain takes up less of the total data length. Additionally, the calibrated parameters had to meet two filtering criteria: 1) the model must converge, and 2) NSE during the calibration period should be greater than 0.7. While we did not conduct validation, we tightened the criterion for the calibration period.

The plant hydraulic properties obtained using the dynamic-window method were analysed through multiple linear regression to examine correlations with the corresponding climate variables. Radiation and temperature were represented by 20-day averages corresponding to the dynamic window, while rainfall was represented by the cumulative precipitation prior to the calibration period, with the cumulative days chosen based on optimal performance in the multiple linear regression model.

3 Results and Discussion

3.1 Pumping test analogue validation results

We successfully simulated the hourly sap-flow rate during the calibration periods. For most periods, the simulated sap flow in Tree 2 closely matched the observed patterns (Fig. 4, column 1), especially the diel variations. We even captured the sudden fluctuations caused by weather, such as radiation reduction due to cloud cover. For example, the calibrated whole-plant hydraulic model reproduced the sudden drops in sap flow at daytime on May 15th (P3 in Fig. 4) and Oct 12th (P7). The NSEs for the Tree 2 calibration periods were higher than 0.8, except for P10 to P12. The simulated sap flow (orange line) had an obvious time lag compared with the observed data in the last periods.

The validation results show that the derived hydraulic properties have good representativeness in the weeks before and after the calibration periods. The hydraulic properties derived during autumn (P1 - P4) effectively reproduced sap-flow rates during autumn and winter (April to July; Fig. 4, column 2). However, the results tended to underestimate sap-flow rates in spring and summer (September to February). Conversely, hydraulic properties derived from summer periods (P5 - P9) exhibited an opposing pattern, resulting in accurate estimation in spring and summer but overestimation during autumn and winter. It is noted that in some early summer calibration periods, the model underestimates sap flow in late summer (P5 - P7) as well. This underestimation is not due to a limitation in maximum hydraulic conductance but rather results from the shape of the vulnerability curve, specifically the relatively high (less negative) Ψ_{50} values derived for these periods. A higher Ψ_{50} indicates greater sensitivity of hydraulic conductance to declining water potential, causing hydraulic conductance to drop rapidly under moderate water stress. This sharp decline in simulated hydraulic conductance effectively limits sap flow in the simulation. The temporal dynamics of Ψ_{50} are analysed in more detail in the next section (see

Fig. 5c). This result indicates that the proposed pumping-test analogue method can derive hydraulic properties with robust seasonal representativeness and capture the presence of seasonal variations in these properties as well. This result is consistent with previous studies in the plant physiology community, who found that the calibrated hydraulic properties in ecological models are not transferable across seasons (Steppe et al., 2008; Baert et al., 2014; Salomón et al., 2017). The NSEs decreased with the extension of the validation period, as expected. The number of days when NSEs were higher than the threshold 0.6 was 50 days or more for most validation periods (Fig. 4, column 3). The validation criterion was set to a required minimum extension of 20 days in the validation period, in addition to the calibration period of 5-7 days. This guarantees that with a week of monitoring data, we can derive plant hydraulic properties that are representative for at least one month. The calibration and validation results of the other two trees confirm the findings for Tree 2 (Fig. S1 & S2).

The derived properties for the three trees based on the three criteria are presented in Table 2. The derived hydraulic properties are considered acceptable for over 50% of the calibration periods. The derived properties that did not meet the criteria were primarily concentrated in January and April; for example, in the period of January 6th, 2019, none of the three trees passed the filtering criteria. This is likely because the simple whole-plant hydraulic model fails under a severe water-stress condition. We have treated the plant as a single capacitor to simplify the model, but realistically, stems contain many capacitors distributed throughout wood and bark with resistors between the wood and bark (Hölttä et al., 2006). Under extreme water stress, the hydraulic resistance between the xylem and phloem likely increases (Baert et al., 2014), effectively preventing the bark from contributing to total capacitance. Hence, capacitance dynamics can behave differently under severe stress than otherwise. The pumping-test analogue requires careful and critical validation under severe water stress. Moreover, it is worth noting that during periods of sufficient water conditions, such as winter in this study, the stem psychrometers are prone to failing (Fig. 2). This may be due to water entering the psychrometer chamber from the ambient environment or sapwood in the wet season. The psychrometer measures water potential based on Peltier cooling; once there is water in the chamber, the stem psychrometer fails to work.

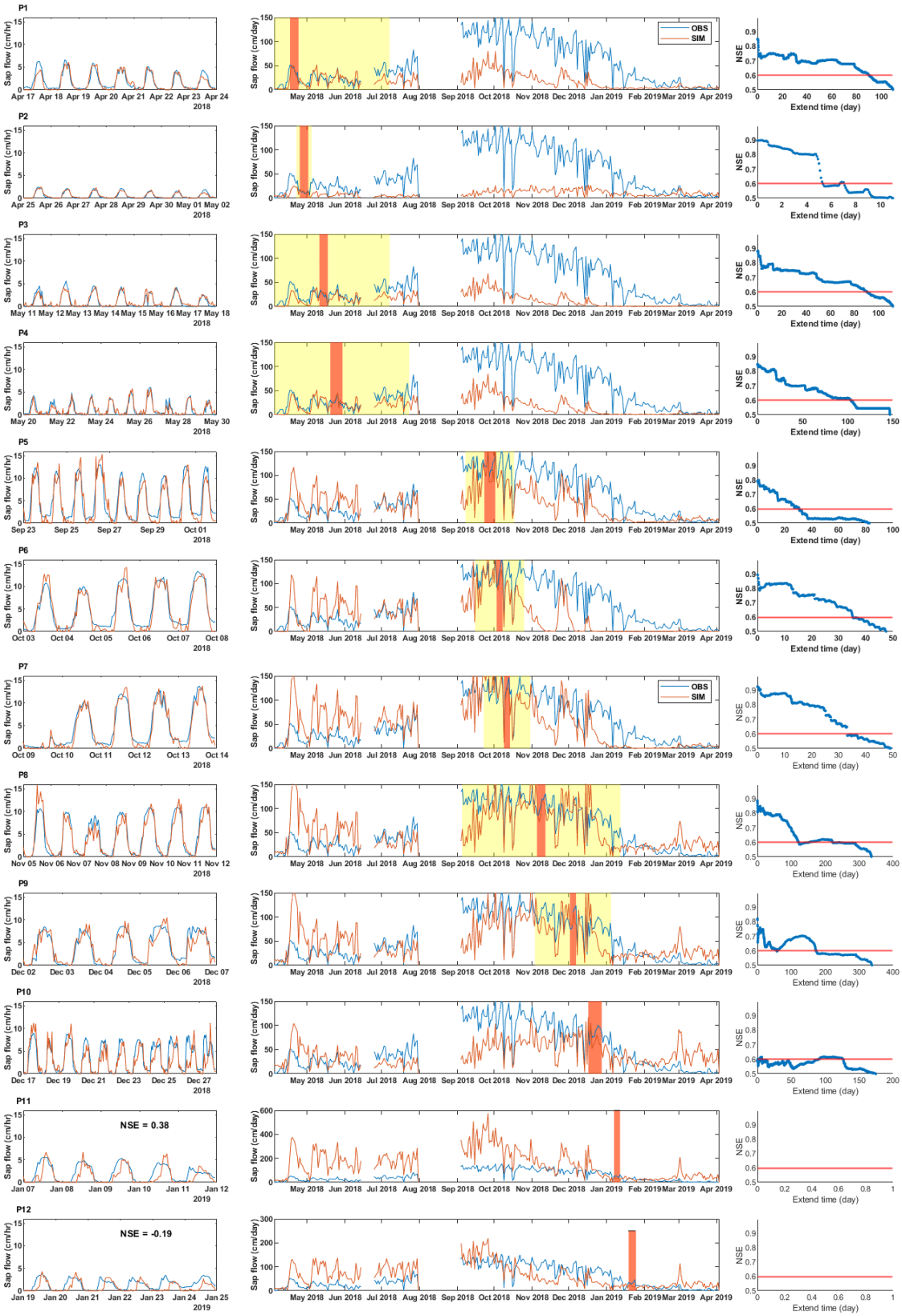

Figure 4: The calibration and validation results on Tree 2. There are twelve calibration periods (P1 – P12) in total. The first column for each period shows the observed (blue) and simulated (orange) hourly sap-flow rate in each calibration period. The second column for each period shows the observed (blue) and simulated (orange) daily sap-flow rate in the whole period. The orange boxes are the calibration periods, and the yellow boxes are the

representative periods with validation NSE larger than 0.6. The third column for each period is the NSE changes with validation periods extending from the calibration periods. The orange line indicates the NSE threshold of 0.6.

Table 2: Filtered results showing whether the estimated hydraulic properties of each tree during specific periods met all three defined criteria. Check mark means that the hydraulic properties of the tree in that period passed the criterion; cross mark means failing the criterion; dash means no measurement data in that period. Criteria 1 is that the NSE must be higher than 0.6 in the calibration period. Criteria 2 is that the extended validation period with NSE higher than 0.6 must be longer than 20 days. Criteria 3 is that the Gelman and Rubin statistics (R_stat) must be lower than 1.2 to confirm the convergence of the MCMC process.

		P1	P2	P3	P4	P5	P6	P7	P8	P9	P10	P11	P12	P13	P14	P15	P16
		17/04/2018	25/04/2018	11/05/2018	20/05/2018	22/09/2018	3/10/2018	9/10/2018	5/11/2018	28/11/2018	17/12/2018	6/01/2019	19/01/2019	9/04/2019	20/05/2019	29/05/2019	15/06/2019
Tree 2	Criteria 1	√	√	√	√	√	√	√	√	√	√	X	X	-	-	-	-
	Criteria 2	√	X	√	√	√	√	√	√	√	√*	-	-	-	-	-	-
	Criteria 3	√	-	√	√	√	√	X	√	√	√	-	-	-	-	-	-
Tree 3	Criteria 1	√	√	-	-	-	-	-	√	√	√	√	√	X	√	√	√
	Criteria 2	√	√	-	-	-	-	-	√	X	√	√	X	-	√	√	X
	Criteria 3	X	√	-	-	-	-	-	√	-	√	X	-	-	√	√	-
Tree 4	Criteria 1	√	-	-	√	√	-	-	-	√	√	√	√	-	-	-	-
	Criteria 2	X	-	-	X	√	-	-	-	√	√	X	X	-	-	-	-
	Criteria 3	X	-	-	-	√	-	-	-	√	√	X	-	-	-	-	-

* *P10 failed the second criterion, strictly, but because the validation NSEs were around 0.6 in more than 50 days, this period was included in the subsequent analysis.*

3.2 Seasonal variation of hydraulic conductance and capacitance

The pumping-test analogue reveals seasonal variations in plant hydraulic properties. The relationship between the estimated hydraulic conductance k_P and plant water potential ψ_P changed across calibration periods, and is therefore time-variant, rather than time-invariant (Fig. 5a). Figures 5b and 5c further illustrate the seasonal variations of two key parameters—maximum hydraulic conductance ($k_{max,25}$) and Ψ_{50}—that control this relationship. The posterior distributions of the maximum hydraulic conductance are very narrow, indicating a low uncertainty of the derived properties (Fig. S3).

The three trees display the same pattern for the maximum hydraulic conductance $k_{max,25}$, with higher values in early spring (September), a gradual decrease from spring to summer (October to January), and a return to higher maximum hydraulic conductance in the following spring and early summer (June 2019) (Fig. 5b). This indicates that the maximum hydraulic conductance $k_{max,25}$ drops as the water stress intensified in the dry season and recovers with root zone moisture replenishment in wet season. Despite April and May being at the transition into the wet season, the maximum hydraulic conductance $k_{max,25}$ stays relatively low. This result indicates that plants and their xylem embolisms need time to recover from the dry season. The three trees also display the same pattern for Ψ_{50}, which decreases from high values (low cavitation resistance) in spring to low values (high resistance) in the dry summer months of Dec-Jan (Fig.5c). This may reflect progressive loss of the most vulnerable conduits as soils dry out and tree water potentials decline.

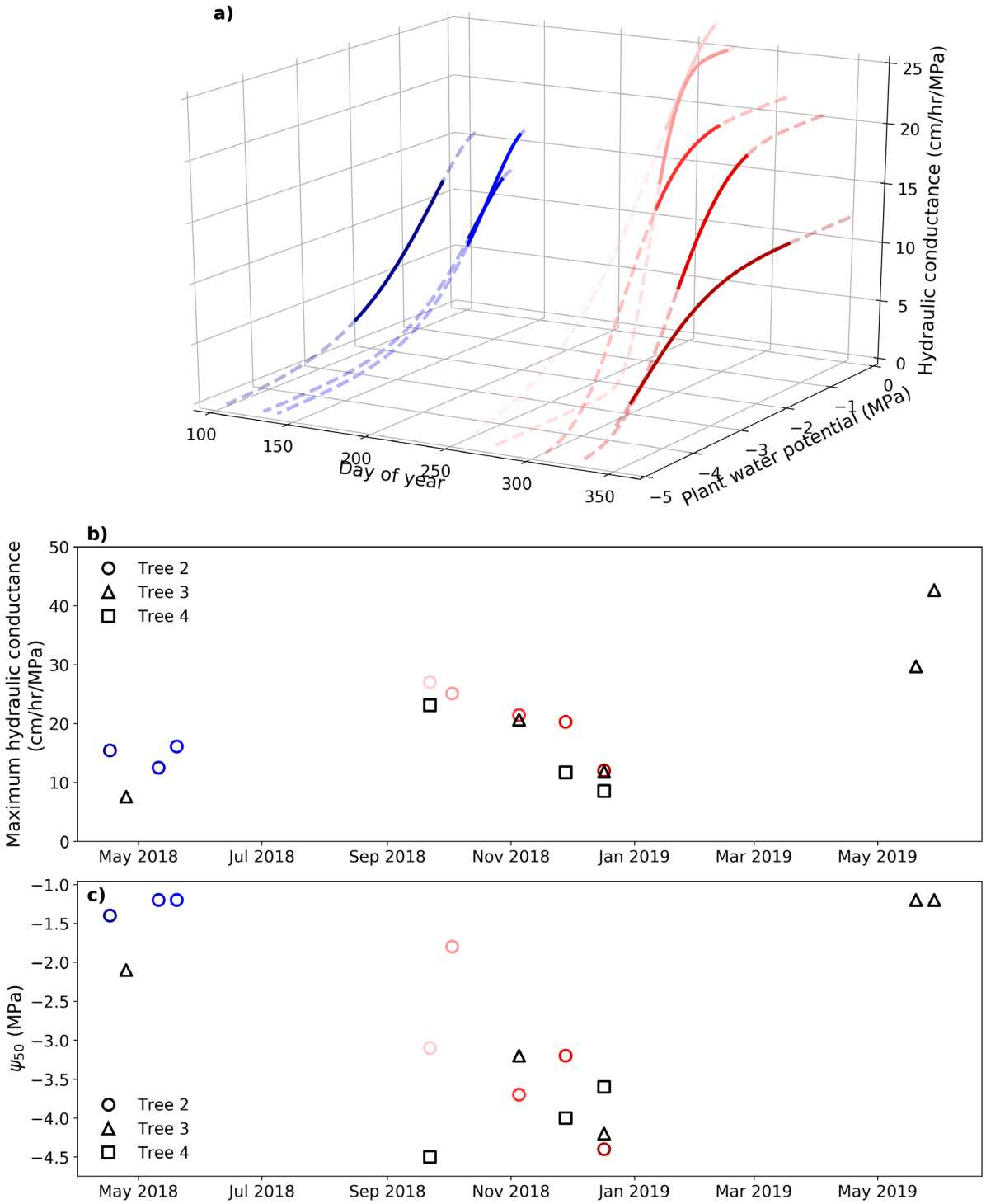

Figure 5: Seasonal variation of hydraulic conductance. (a) Derived hydraulic conductance of Tree 2 with varying plant water potentials over the calibration periods. Cool colours (e.g., blue) represent the wet season, while warm colours (e.g., red) represent the dry season. The dashed lines show water potentials from -5 to 0 MPa, while the solid lines show the water potentials measured during the calibration periods. (b) The seasonal variation of the derived maximum hydraulic conductance ($k_{max,25}$) of all the trees. (c) The seasonal variation of the derived Ψ50 of all the trees.

The maximum hydraulic capacitance shows a similar pattern to the maximum hydraulic conductance, with higher values in spring and lower values in autumn. It gradually decreased with an intensification of water stress (Fig. 6a). However, there is an interesting pattern: in November and December, when water stress was

developing, the maximum hydraulic capacitance was relatively small, but the hydraulic capacitance was high where the water potential was low (about -3 MPa; the dark red lines in Fig. 6a). A similar pattern existed for the other two trees. The seasonal changes in plant hydraulic capacitance and conductance, derived by the pumping-test analogue, indicate that in the wet season (with plenty of rainfall but low transpiration demand), the plants mainly transpire water taken up directly from the soil, and their internal storage is not fully used. In contrast, during the dry season, a greater proportion of the stored water is used to meet the plant transpiration demand. This suggests that the water storage of trees is more important for transpiration at low water potentials during the dry season than at higher water potentials in the wet season. The effective hydraulic capacitance is not only determined by their intrinsic properties but also by hydrometeorological conditions, that plant effective hydraulic capacitance differs significantly during dry and wet seasons. We conclude these changes of effective hydraulic capacitance from a model-inversion perspective; more direct measurements of plant water storage across seasons are needed to validate these findings.

The pumping-test analogue, based on a whole-plant approach to derive plant hydraulic properties from the relationship between plant water use and water status, differs significantly from traditional laboratory-based measurement methods in the plant physiology community. Despite this distinction, we have arrived at the same conclusion as seen in previous studies: plant hydraulic properties exhibit seasonal plasticity, and we have shown more continuous data to support this conclusion. The specific seasonal changes in hydraulic conductance that we derived ($k_{max,25}$ in Fig. 5b and Ψ_{50} in Fig.5c) align with most existing studies. There are some potential mechanisms to interpret seasonal plasticity of hydraulic conductance. The most straightforward one is that as summer drought intensifies, plants may produce more cavitation-resistant vessels, while in the wetter winter months, they may form larger, more conductive but more vulnerable vessels—thus maximizing hydraulic efficiency and growth. Therefore, it is reasonable to speculate that vessel development and repair processes are closely linked to seasonal plasticity in hydraulic properties. Also, in a population of xylem vessels, the most vulnerable ones will cavitate first, leaving behind a reduced number of xylem vessels with lower conductance but greater resistance to cavitation (more negative Ψ_{50}). Another possible mechanism is that seasonal shifts in plant hydraulic properties may be influenced by changes in xylem sap composition. Recent research has shown that lipids present in xylem sap can alter the sap's surface tension (Schenk et al., 2018; Yang et al., 2020), which may potentially affect hydraulic efficiency and safety. While these potential mechanisms remain to be directly tested, they offer potential directions for understanding the mechanism of the seasonal plasticity of plant hydraulics. Future research combining detailed physiological measurements with modelling efforts could help elucidate the biological mechanisms underlying these patterns.

While the seasonal plasticity of maximum effective hydraulic capacitance ($C_{\max}$) is reported for the first time here, the results make sense because the release and recovery of stored plant water are also dependent on the hydraulic conductivity between xylem and storage, which varies seasonally (Hölttä et al., 2006). A higher hydraulic conductivity may facilitate more efficient mobilization of stored water, leading to higher effective capacitance. In addition, seasonal structural changes in plants may further influence hydraulic capacitance. During the wet season, the formation of sapwood and bark tissues may expand the plant's internal water storage capacity, thereby affecting capacitance. It should be noted, however, that we currently lack data on seasonal phenological changes—such as xylem growth, phloem development, or variation in leaf area—for drooping sheoak. Therefore, the mechanisms discussed above remain hypothetical and need further investigation.

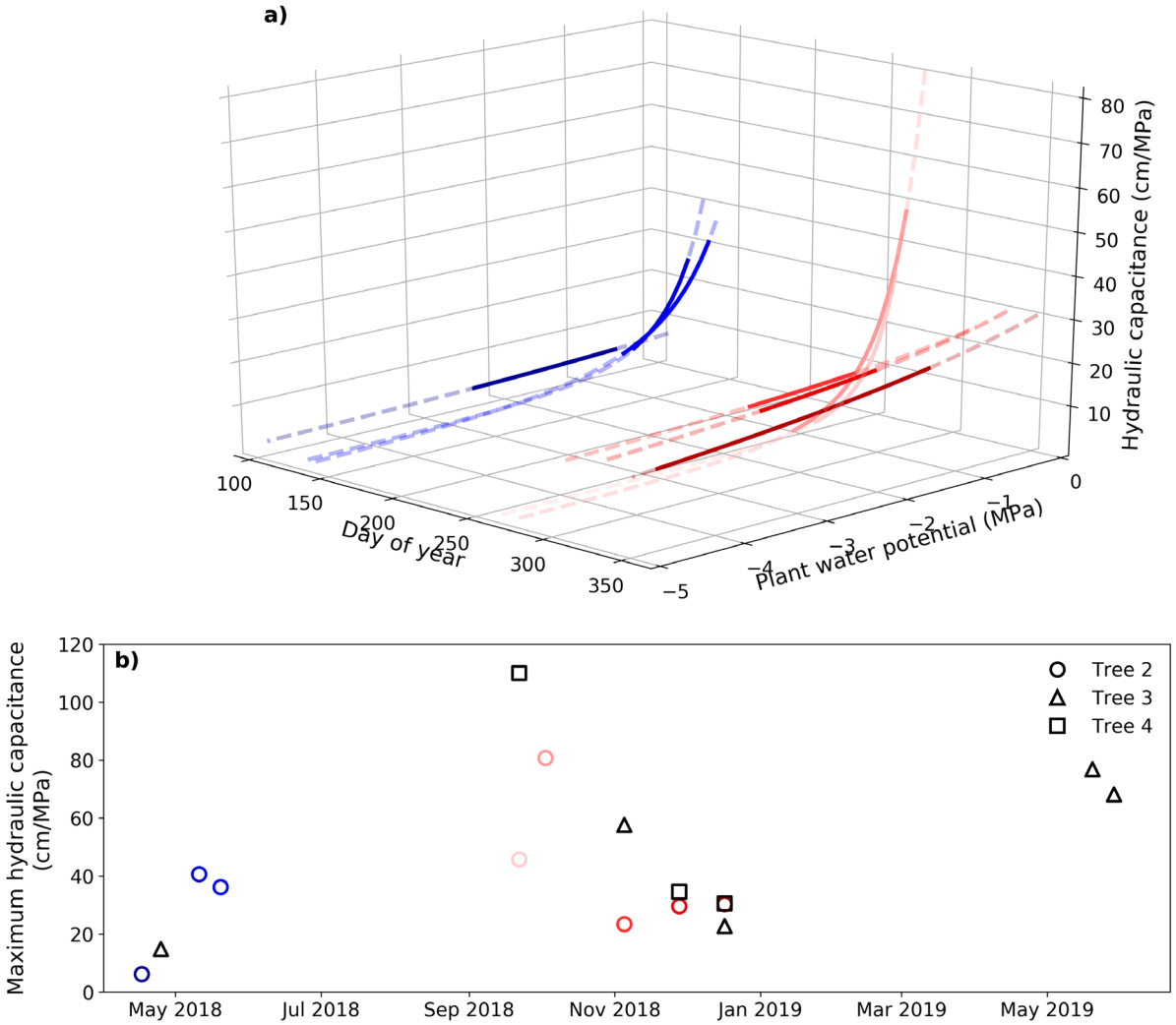

Figure 6: Seasonal variation of hydraulic capacitance. (a) Derived hydraulic capacitance of Tree 2 with varying plant water potentials over the calibration periods. The dashed lines show water potentials from -5 to 0 MPa, while the solid lines show the water potentials measured during the calibration periods. Cool colours (e.g., blue) represent the wet season, while warm colours (e.g., red) represent the dry season. (b) The seasonal variation of the derived maximum hydraulic capacitance (C_{max}) of all the trees.

3.3 Insights from the derived time-varying plant hydraulic properties

By applying calibration and validation methods during dry spells, we identified that the pumping-test analogue is capable of deriving key plant hydraulic properties and reveal that these properties exhibit seasonal plasticity. Building on this result, we explored the plant hydraulic properties near-continuously. Figure 7 presents the plant hydraulic properties ($k_{max,25}$, Ψ_{50}, and C_{max}) derived using the dynamic-window method. After filtering (calibration NSE > 0.7), the time range of the representative plant hydraulic properties is consistent with the range obtained from the no-rain periods. Except for the period from January to April 2019, most other periods pass the filtering criteria. This further supports our previous conclusion that the failure of the method for this period was not incidental. During other periods, the seasonal variation pattern of plant hydraulic properties is consistent with the previous results shown in Fig. 5. Maximum hydraulic conductance $k_{max,25}$ decreased during the dry season, especially from October to December 2018 (as shown in Fig. 7), while Ψ_{50} became more

negative as the dry season progressed. Figure 7 also shows the variation in root-zone water potential, indicating that changes in $k_{max,25}$ and Ψ_{50} closely correlate with changes in root-zone water potential. During the dry season, both $k_{max,25}$ and Ψ_{50} decreased as the root-zone gradually dried out; with replenishment from rainfall or irrigation, these values increased accordingly. Moreover, the increase in plant hydraulic properties slightly lagged the recovery of root-zone water potential (Fig. 7), suggesting that plants require time to respond to root-zone moisture replenishment. This phenomenon is reasonable and further validates the reliability of the derived plant hydraulic properties.

As for C_{max}, its variation generally follows the trend shown in Figure 6b, where it was high in spring, decreased as summer progresses, stayed low in autumn, and likely gradually increased through winter to spring. As mentioned earlier, effective hydraulic capacitance is influenced not only by the plant water status but also by the atmospheric water demand. It peaked in spring when both root-zone water supply and atmospheric demand for transpiration was high. In winter, despite abundant water supply, low water demand resulted in a relatively small maximum effective hydraulic capacitance, as transpiration primarily relies on water uptake from the roots, with limited contribution from stored water. As water demand increased in spring, C_{max} rose. As the dry season progressed, the root zone moisture was depleted, leading to a reduction in C_{max}. The peak observed in January 2019 (inset in Fig. 7c), after an irrigation event, was due to a rapid replenishment of root-zone water combined with high daytime transpiration demand. At night, the plants absorbed significant amounts of water from the root zone into their storage, and with high daytime transpiration demand, the refilled water was quickly transpired during the day. This combination resulted in an exceptionally high C_{max} value.

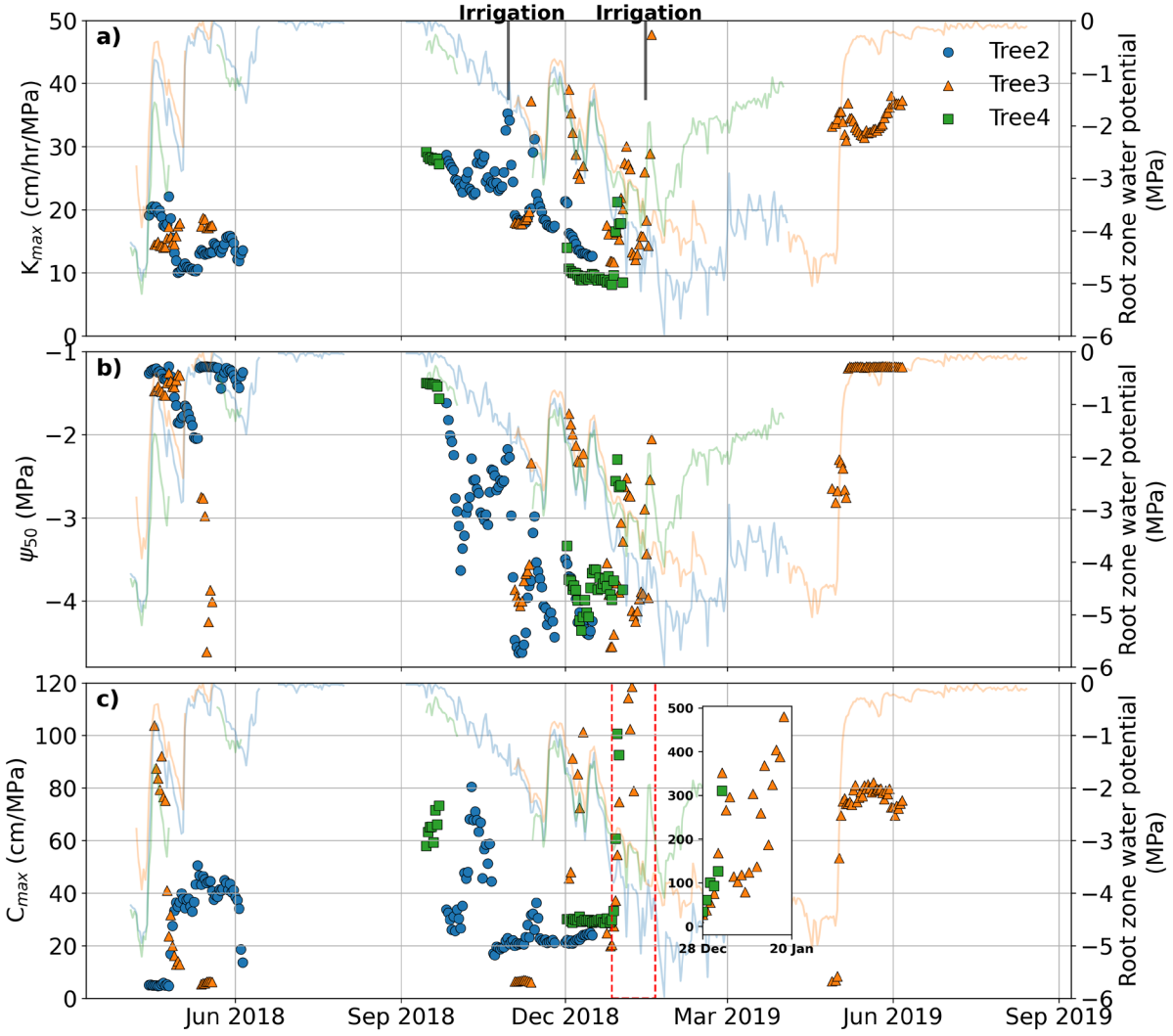

Figure 7: Derived hydraulic properties from April 2018 to July 2019. (a) Maximum hydraulic conductance, (b) Ψ_{50}, and (c) maximum effective hydraulic capacitance were derived based on 20-days calibration periods and only those properties that pass the validation criteria are presented here. The inset in panel (c) highlights the rapid increase in C_{max}, reaching 500 cm/MPa following irrigation. The data points represent the midpoint of each 20-day period. The lines show the root-zone water-potential dynamics.

3.4 Relations between seasonal variations of plant hydraulic properties and climate variables

The pumping-test analogue has provided a large amount of plant hydraulic property data, which enables analyses and research that were previously difficult to conduct. This paper presents two preliminary attempts to apply the pumping-test analogue. The first attempt is to explore the relationship between plant hydraulic properties and climate variables. Plant traits and growth are closely linked to climate conditions, with the primary climate factors being moisture, radiation, and temperature, and the key climate variables differing depending on the plant species and the climatic zone (Nemani et al., 2003; Seddon et al., 2016). The correlation between hydraulic properties and climate variables for drooping sheoak under a Mediterranean climate is shown in Table 3. Precipitation, radiation, and temperature can partially explain the seasonal variation in plant hydraulic properties, with the best regression observed for Ψ_{50} explaining 61% of the variation. Precipitation is a significant predictor variable in the regression models for plant hydraulic properties in all three trees, and the effect is positive, indicating that plant hydraulic properties increase as precipitation increases. This finding aligns with the trend observed in Fig. 7, where plant hydraulic properties and root zone water potential exhibit

similar changes. This suggests that, under a Mediterranean climate, precipitation conditions are the primary determinant of the drooping sheoak's hydraulic property variations. Regarding $k_{max,25}$, temperature is a significant predictor with a negative effect. Radiation is not a significant predictor in the regression. In Mediterranean climates, temperatures are low in the wet season and high in the dry season, so high temperatures during the dry season exacerbate the reduction in $k_{max,25}$. In terms of Ψ_{50}, radiation is a predictor with a negative effect, and temperature has a positive effect. This suggests that high radiation during the dry season causes a reduction in Ψ_{50}, leading plants to adopt a more conservative hydraulic strategy, while temperature has the opposite effect, promoting an increase in Ψ_{50}. In contrast, no significant relationships between C_{max} and either temperature or radiation are found by the regression. It is important to emphasize that this is a preliminary trial, based on a limited monitoring duration from a single species within a specific climate zone. The relationship between plant hydraulic properties and climate variables is complex and requires further analysis using longer-term sap-flow and stem water-potential data, as well as additional related data, such as phenology. Additionally, there is a significant correlation between the three climate variables selected in this study, and future research should aim to isolate the independent effects of each climate variable on hydraulic properties.

Table 3: Multiple linear regression models for the relationship between plant hydraulic properties and climate variables.

	P_{105}	R_{20}	T_{20}	Intercept	R^2
$k_{max,25}$	**0.038**	0.053	**-1.23**	37.18	0.27
(p-value)	0.000	0.77	0.001	0.000	
Ψ_{50}	**0.0055**	**-0.21**	**0.14**	-2.51	0.61
(p-value)	0.001	0.000	0.000	0.000	
C_{max}	0.15	-0.59	1.97	6.64	0.02
(p-value)	0.09	0.55	0.32	0.82	

* *Note: Each model's first row shows the regression coefficients (slopes), while the second row displays the corresponding P-values for each climate variable. The intercepts and R^2 values are also presented.*

3.5 Seasonal variation of the trade-off between hydraulic efficiency and safety

The second attempt to apply the pumping-test analogue is to explore the relationship between plant hydraulic efficiency and safety. In theory, higher hydraulic efficiency is associated with relatively less-safe hydraulic strategies. A global metanalysis (Gleason et al., 2016) confirmed this trade-off between hydraulic efficiency and safety across the world's woody plant species, but it is not strong. Trade-offs have also been observed between different parts of a plant within the same tree (Domec et al., 2006; Meinzer et al., 2010). In this study, we attempted to investigate whether a trade-off between hydraulic efficiency (represented by $k_{max,25}$) and safety (represented by Ψ_{50}) exists within individual plants across different seasons, as we know that plant hydraulic efficiency and safety can vary seasonally. Figure 8 illustrates a relationship between Ψ_{50} and $k_{max,25}$: as the dry season progressed, plant hydraulic efficiency declined, and the hydraulic strategy shifted to be more conservative and safety-oriented (with Ψ_{50} tending to more negative values). In contrast, with the start of the rainy season, hydraulic efficiency improved, and the hydraulic strategy shifted to a more efficiency-oriented mode (with Ψ_{50} shifting to less negative values). This pattern suggests a potential trade-off between hydraulic efficiency and safety within individual plants. It is noteworthy that although the Ψ_{50} values in May 2018 (circled in Fig. 9) were similar to those in the same period of 2019, $k_{max,25}$ in 2018 was much lower than in 2019. Two possible explanations for this difference are: first, the plant experienced significant sapwood growth from 2018 to 2019, resulting in improved hydraulic efficiency; second, the plant experienced higher water stress during

2017-2018 compared to 2018-2019. This second explanation is supported by Figure 4c, which shows that cumulative rainfall in May 2018 was approximately 50 mm, compared to around 100 mm in May 2019. The lower rainfall in 2018 may have led to more severe cavitation, resulting in a delayed recovery in hydraulic efficiency at the start of the rainy season. This result is further supported by the stem water potential in April-May 2018, which was lower than during the same period of 2019. The version with standard deviation of Fig.8 is included in Fig. S6.

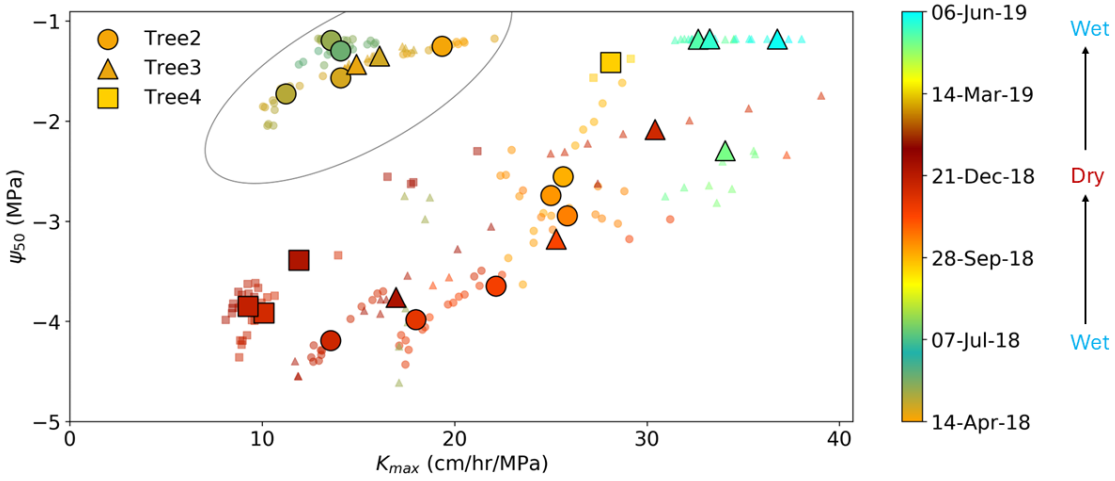

Figure 8: Relationship between Ψ_{50} and $k_{max,25}$ for individual trees. Small dots represent hydraulic properties derived from 20-day dynamic windows, while larger symbols indicate the mean values of every ten consecutive points to clarify overall trends. The oval includes the points from autumn 2018 and the explanations for the deviations of these points are provided in Section 3.5. The colour bar represents the continuous date across the full observation period. Warm colours generally correspond to the dry season, while cool colours represent the wet season. The colour bar was designed to distinguish between 2018 and 2019, hence the slight differences in colour for the same calendar days across years.

Based on the above results (Fig. 5-8), Figure 9 illustrates a generalized schematic of plant hydraulic responses of drooping sheoak to water supply and demand under a Mediterranean climate. This schematic summarizes the expected seasonal variations in key hydraulic properties in response to changes in water availability and atmospheric demand. Water supply (blue line) and water demand (orange line) represent the typical seasonal dynamics in a Mediterranean climate, where water supply is highest during wetter seasons and decreases as the dry season progresses, while water demand follows an inverse pattern, peaking during warmer months. In response to these environmental drivers, the lower three curves illustrate the seasonal dynamics of plant hydraulic efficiency, safety, and buffer. In this study, plant hydraulic efficiency, safety, and buffer are represented by $k_{max,25}$, - Ψ_{50}, C_{max}, respectively. Plant hydraulic efficiency generally follows changes in water supply, and plant hydraulic safety shows the opposite pattern—higher hydraulic efficiency corresponds to lower hydraulic safety (Fig. 8). While plant hydraulic buffer (represented by C_{max}) responds to both water supply and demand. When either supply or demand is low, plant hydraulic buffer remains limited. In contrast, it peaks when both supply and demand are high. This generalized schematic help illustrate how hydraulic properties shift in response to seasonal variations in water supply and demand, providing insights into plant water-use strategies under a Mediterranean climate.

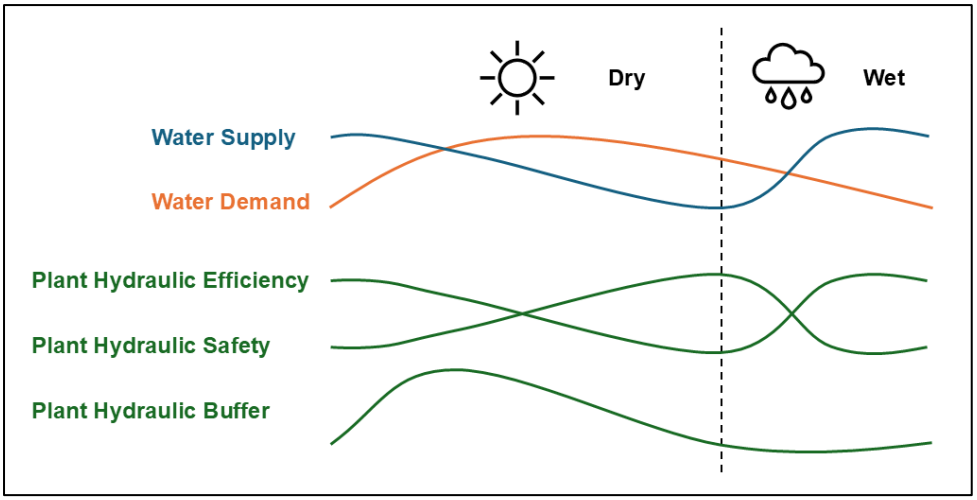

Figure 9: Generalized schematic of plant hydraulic responses in drooping sheoak (*Allocasuarina verticillata*) to water supply and demand under a Mediterranean climate. In this study, plant hydraulic efficiency, safety, and buffer are represented by $k_{max,25}$, $-\Psi_{50}$, C_{max}, respectively. The dry season in Adelaide is from September to April, which is longer than the wet season.

3.6 Opportunities arising from the pumping-test analogue

The two attempts to apply the pumping-test analogue in section 3.4 and 3.5 highlight the future application potential of the pumping-test analogue. Compared with the current laboratory methods, the pumping-test analogue estimates whole-plant parameters, which can be directly applied in models. The method is based on automatic monitoring data, specifically stem water potential and sap flow, and the equipment only needs to be installed once and maintained regularly, which greatly reduces the workload. In addition, the pumping-test analogue is non-destructive, reducing the damage to the plant and the differences caused by sampling on different branches. Additionally, the increasing number of plant water-potential and sap-flow datasets make the application of the pumping-test analogue increasingly feasible.

The near-continuous plant hydraulic property predictions provided by the pumping-test analogue can be used for plant hydraulic research that was previously limited by data availability. It also offers a new possibility for parameterizing plant hydraulic processes in land-surface models. As mentioned in the introduction, seasonal variations of plant hydraulic properties have been reported within the plant physiology community; however, its application in hydrological and land-surface modelling is still rare. The pumping-test analogue could serve as a potential approach to represent and parameterize the seasonal plasticity of plant hydraulic properties in numerical hydrological models.

In short, the pumping-test analogue method is easy to implement, making it suitable for estimating plant hydraulic parameters and their ranges, with potential application to hydrologic models. Due to its easy implementation, it is possible to use the pumping-test analogue at different locations or on different species to conduct spatial and inter- and intra-species analysis, which may allow us to build a comprehensive understanding of plant hydraulic property variation.

4 Conclusions

We developed a new, in-situ method to derive representative whole-plant hydraulic properties through a pumping-test analogue. We developed and applied the pumping-test analogue method on *Allocasuarina*

verticillata and revealed the seasonal variation of maximum hydraulic conductance, effective capacitance, and hydraulic vulnerability. The hydraulic properties obtained through this method from one-week monitoring is suitable for modelling plant hydraulic processes for at least one month, except during the periods of severe water stress. This method provides new evidence for the seasonal plasticity of plant hydraulic properties and provides insights into how the hydraulic properties in drooping sheoak vary seasonally under Mediterranean climate.

In this study, we also used near-continuous hydraulic properties derived by the pumping-test analogue to explore the relationship between plant hydraulic properties and climate variables, as well as the trade-off between hydraulic efficiency and safety within individual plants across different seasons. These preliminary findings indicate that it is feasible to estimate plant hydraulic properties under various conditions. Consequently, this method enables a comprehensive understanding of the variations in plant hydraulic properties and provides the potential for accurate estimation of plant hydraulic parameters for land-surface modelling. An accurate description of plant hydraulics in land-surface models will help decrease the uncertainty of the water and carbon flux simulation.

Acknowledgments

Craig Simmons from The University of Newcastle, Australia is greatly appreciated for providing comments and suggestions at an early stage of this research. Zijuan Deng, Yifei Zhou, Na Liu and Zidong Luo assisted with field data collection. Zhechen Zhang appreciates the financial support from the China Scholarship Council. Zhechen Zhang and Huade Guan gratefully acknowledge the Jack Kimmel International Grant from the TREE Fund. We also thank the anonymous reviewer and Jessica Guo for their constructive and insightful comments, which greatly improved the quality of this manuscript.

Data and code availability

Software, including Sap Flow Tool (https://ictinternational.com/manuals-and-brochures/sfm1x-sap-flow-meter/), Matlab R2012b (https://au.mathworks.com/products/matlab.html), and Python is used to generate data sets, models, and figures. All the data was submitted to PSInet for public access.

Author contribution

ZZ - Formal analysis, Methodology, Investigation, Visualization, Writing – original draft preparation; HG – Conceptualization, Investigation, Resources, Supervision, Writing – review & editing; EV – Methodology, Writing – review & editing; KS – Methodology, Writing – review & editing; OB - Writing – review & editing

Competing interests

The authors declare that they have no conflict of interest.

References

Anderegg, W. R. L. and Callaway, E. S.: Infestation and Hydraulic Consequences of Induced Carbon Starvation, Plant Physiology, 159, 1866-1874, 10.1104/pp.112.198424, 2012.

Anderegg, W. R. L. and Meinzer, F. C.: Wood Anatomy and Plant Hydraulics in a Changing Climate, 10.1007/978-3-319-15783-2_9, 2015.

Baert, A., De Schepper, V., and Steppe, K.: Variable hydraulic resistances and their impact on plant drought response modelling, Tree Physiology, 35, 439-449, 10.1093/treephys/tpu078, 2014.

Baig, F., Sherif, M., and Faiz, M. A.: Quantification of Precipitation and Evapotranspiration Uncertainty in Rainfall-Runoff Modeling, Hydrology, 9, 51, 2022.

Barros, F. d. V., Bittencourt, P. R. L., Brum, M., Restrepo-Coupe, N., Pereira, L., Teodoro, G. S., Saleska, S. R., Borma, L. S., Christoffersen, B. O., Penha, D., Alves, L. F., Lima, A. J. N., Carneiro, V. M. C., Gentine, P., Lee, J.-E., Aragão, L. E. O. C., Ivanov, V., Leal, L. S. M., Araujo, A. C., and Oliveira, R. S.: Hydraulic traits explain differential responses of Amazonian forests to the 2015 El Niño-induced drought, New Phytologist, 223, 1253-1266, https://doi.org/10.1111/nph.15909, 2019.

Bohrer, G., Mourad, H., Laursen, T. A., Drewry, D., Avissar, R., Poggi, D., Oren, R., and Katul, G. G.: Finite element tree crown hydrodynamics model (FETCH) using porous media flow within branching elements: A new representation of tree hydrodynamics, Water Resources Research, 41, https://doi.org/10.1029/2005WR004181, 2005.

Buckley, T. N. and Roberts, D. W.: DESPOT, a process-based tree growth model that allocates carbon to maximize carbon gain, Tree Physiology, 26, 129-144, 10.1093/treephys/26.2.129, 2006.

Christoffersen, B. O., Gloor, M., Fauset, S., Fyllas, N. M., Galbraith, D. R., Baker, T. R., Kruijt, B., Rowland, L., Fisher, R. A., Binks, O. J., Sevanto, S., Xu, C., Jansen, S., Choat, B., Mencuccini, M., McDowell, N. G., and Meir, P.: Linking hydraulic traits to tropical forest function in a size-structured and trait-driven model (TFS v.1-Hydro), Geosci. Model Dev., 9, 4227-4255, 10.5194/gmd-9-4227-2016, 2016.

Chuang, Y.-L., Oren, R., Bertozzi, A. L., Phillips, N., and Katul, G. G.: The porous media model for the hydraulic system of a conifer tree: Linking sap flux data to transpiration rate, Ecological Modelling, 191, 447-468, https://doi.org/10.1016/j.ecolmodel.2005.03.027, 2006.

Cochard, H., Martin, R., Gross, P., and Bogeat-Triboulot, M. B.: Temperature effects on hydraulic conductance and water relations of Quercus robur L, Journal of Experimental Botany, 51, 1255-1259, 10.1093/jexbot/51.348.1255, 2000.

Cowan, I. R.: Transport of Water in the Soil-Plant-Atmosphere System, Journal of Applied Ecology, 2, 221-239, 10.2307/2401706, 1965.

Deng, Z., Guan, H., Hutson, J., Forster, M. A., Wang, Y., and Simmons, C. T.: A vegetation-focused soil-plant-atmospheric continuum model to study hydrodynamic soil-plant water relations, Water Resources Research, 53, 4965-4983, https://doi.org/10.1002/2017WR020467, 2017.

Dingman, S. L.: Physical hydrology, Waveland press2015.

Domec, J.-C., Lachenbruch, B., and Meinzer, F. C.: Bordered pit structure and function determine spatial patterns of air-seeding thresholds in xylem of Douglas-fir (Pseudotsuga menziesii; Pinaceae) trees, American Journal of Botany, 93, 1588-1600, https://doi.org/10.3732/ajb.93.11.1588, 2006.

Feng, F., Wagner, Y., Klein, T., and Hochberg, U.: Xylem resistance to cavitation increases during summer in Pinus halepensis, Plant, Cell & Environment, 46, 1849-1859, https://doi.org/10.1111/pce.14573, 2023.

Gelman, A. and Rubin, D. B.: Inference from iterative simulation using multiple sequences, Statistical science, 7, 457-472, 1992.

Gleason, S. M., Westoby, M., Jansen, S., Choat, B., Hacke, U. G., Pratt, R. B., Bhaskar, R., Brodribb, T. J., Bucci, S. J., Cao, K.-F., Cochard, H., Delzon, S., Domec, J.-C., Fan, Z.-X., Feild, T. S., Jacobsen, A. L., Johnson, D. M., Lens, F., Maherali, H., Martínez-Vilalta, J., Mayr, S., McCulloh, K. A., Mencuccini, M., Mitchell, P. J., Morris, H., Nardini, A., Pittermann, J., Plavcová, L., Schreiber, S. G., Sperry, J. S., Wright, I. J., and Zanne, A. E.: Weak tradeoff between xylem safety and xylem-specific hydraulic efficiency across the world's woody plant species, New Phytologist, 209, 123-136, https://doi.org/10.1111/nph.13646, 2016.

Heggen, R. J.: Thermal Dependent Physical Properties of Water, Journal of Hydraulic Engineering, 109, 298-302, doi:10.1061/(ASCE)0733-9429(1983)109:2(298), 1983.

Hölttä, T., Vesala, T., Sevanto, S., Perämäki, M., and Nikinmaa, E.: Modeling xylem and phloem water flows in trees according to cohesion theory and Münch hypothesis, Trees, 20, 67-78, 10.1007/s00468-005-0014-6, 2006.

Huang, C.-W., Domec, J.-C., Ward, E. J., Duman, T., Manoli, G., Parolari, A. J., and Katul, G. G.: The effect of plant water storage on water fluxes within the coupled soil–plant system, New Phytologist, 213, 1093-1106, https://doi.org/10.1111/nph.14273, 2017.

Hunt, E. R., Running, S. W., and Federer, C. A.: Extrapolating plant water flow resistances and capacitances to regional scales, Agricultural and Forest Meteorology, 54, 169-195, https://doi.org/10.1016/0168-1923(91)90005-B, 1991.

Jacobsen, A. L., Pratt, R. B., Davis, S. D., and Ewers, F. W.: Cavitation resistance and seasonal hydraulics differ among three arid Californian plant communities, Plant, Cell & Environment, 30, 1599-1609, https://doi.org/10.1111/j.1365-3040.2007.01729.x, 2007.

Jiménez-Rodríguez, C. D., Sulis, M., and Schymanski, S.: The Role of the Intraspecific Variability of Hydraulic Traits for Modeling the Plant Water Use in Different European Forest Ecosystems, Journal of Advances in Modeling Earth Systems, 16, e2022MS003494, https://doi.org/10.1029/2022MS003494, 2024.

Kennedy, D., Swenson, S., Oleson, K. W., Lawrence, D. M., Fisher, R., Lola da Costa, A. C., and Gentine, P.: Implementing Plant Hydraulics in the Community Land Model, Version 5, Journal of Advances in Modeling Earth Systems, 11, 485-513, https://doi.org/10.1029/2018MS001500, 2019.
Kolb, K. J. and Sperry, J. S.: Transport constraints on water use by the Great Basin shrub, Artemisia tridentata, Plant, Cell & Environment, 22, 925-935, https://doi.org/10.1046/j.1365-3040.1999.00458.x, 1999.
Li, L., Yang, Z.-L., Matheny, A. M., Zheng, H., Swenson, S. C., Lawrence, D. M., Barlage, M., Yan, B., McDowell, N. G., and Leung, L. R.: Representation of Plant Hydraulics in the Noah-MP Land Surface Model: Model Development and Multiscale Evaluation, Journal of Advances in Modeling Earth Systems, 13, e2020MS002214, https://doi.org/10.1029/2020MS002214, 2021.
Li, Z., Wang, C., Luo, D., Hou, E., and Ibrahim, M. M.: Leaf-branch vulnerability segmentation occurs all year round for three temperate evergreen tree species, Plant Physiology and Biochemistry, 197, 107658, https://doi.org/10.1016/j.plaphy.2023.107658, 2023.
Liu, N., Deng, Z., Wang, H., Luo, Z., Gutiérrez-Jurado, H. A., He, X., and Guan, H.: Thermal remote sensing of plant water stress in natural ecosystems, Forest Ecology and Management, 476, 118433, https://doi.org/10.1016/j.foreco.2020.118433, 2020a.
Liu, Y., Holtzman, N. M., and Konings, A. G.: Global ecosystem-scale plant hydraulic traits retrieved using model–data fusion, Hydrol. Earth Syst. Sci., 25, 2399-2417, 10.5194/hess-25-2399-2021, 2021.
Liu, Y., Kumar, M., Katul, G. G., Feng, X., and Konings, A. G.: Plant hydraulics accentuates the effect of atmospheric moisture stress on transpiration, Nature Climate Change, 10, 691-695, 10.1038/s41558-020-0781-5, 2020b.
Liu, Y., Parolari, A. J., Kumar, M., Huang, C.-W., Katul, G. G., and Porporato, A.: Increasing atmospheric humidity and CO_2 concentration alleviate forest mortality risk, Proceedings of the National Academy of Sciences, 114, 9918-9923, doi:10.1073/pnas.1704811114, 2017.
Loritz, R., Bassiouni, M., Hildebrandt, A., Hassler, S. K., and Zehe, E.: Leveraging sap flow data in a catchment-scale hybrid model to improve soil moisture and transpiration estimates, Hydrol. Earth Syst. Sci., 26, 4757–4771, https://doi.org/10.5194/hess-26-4757-2022, 2022.
Loustau, D., Domec, J.-C., and Bosc, A.: Interpreting the variations in xylem sap flux density within the trunk of maritime pine (Pinus pinaster Ait.): application of a model for calculating water flows at tree and stand levels, Annales des Sciences Forestieres, 29-46,
Lu, Y., Sloan, B., Thompson, S. E., Konings, A. G., Bohrer, G., Matheny, A., and Feng, X.: Intra-Specific Variability in Plant Hydraulic Parameters Inferred From Model Inversion of Sap Flux Data, Journal of Geophysical Research: Biogeosciences, 127, e2021JG006777, https://doi.org/10.1029/2021JG006777, 2022.
Luo, Z., Deng, Z., Singha, K., Zhang, X., Liu, N., Zhou, Y., He, X., and Guan, H.: Temporal and spatial variation in water content within living tree stems determined by electrical resistivity tomography, Agricultural and Forest Meteorology, 291, 108058, https://doi.org/10.1016/j.agrformet.2020.108058, 2020.
Marshall, T. J., Holmes, J. W., and Rose, C. W.: Soil physics, Cambridge university press1996.
Matheny, A. M., Mirfenderesgi, G., and Bohrer, G.: Trait-based representation of hydrological functional properties of plants in weather and ecosystem models, Plant Diversity, 39, 1-12, https://doi.org/10.1016/j.pld.2016.10.001, 2017a.
Matheny, A. M., Fiorella, R. P., Bohrer, G., Poulsen, C. J., Morin, T. H., Wunderlich, A., Vogel, C. S., and Curtis, P. S.: Contrasting strategies of hydraulic control in two codominant temperate tree species, Ecohydrology, 10, e1815, https://doi.org/10.1002/eco.1815, 2017b.
Meinzer, F. C., McCulloh, K. A., Lachenbruch, B., Woodruff, D. R., and Johnson, D. M.: The blind men and the elephant: the impact of context and scale in evaluating conflicts between plant hydraulic safety and efficiency, Oecologia, 164, 287-296, 10.1007/s00442-010-1734-x, 2010.
Mencuccini, M.: Hydraulic constraints in the functional scaling of trees, Tree Physiology, 22, 553-565, 10.1093/treephys/22.8.553, 2002.

Nemani, R. R., Keeling, C. D., Hashimoto, H., Jolly, W. M., Piper, S. C., Tucker, C. J., Myneni, R. B., and Running, S. W.: Climate-Driven Increases in Global Terrestrial Net Primary Production from 1982 to 1999, Science, 300, 1560-1563, doi:10.1126/science.1082750, 2003.

Novick, K. A., Ficklin, D. L., Baldocchi, D., Davis, K. J., Ghezzehei, T. A., Konings, A. G., MacBean, N., Raoult, N., Scott, R. L., Shi, Y., Sulman, B. N., and Wood, J. D.: Confronting the water potential information gap, Nature Geoscience, 15, 158-164, 10.1038/s41561-022-00909-2, 2022.

Ogle, K., Barber, J. J., Willson, C., Thompson, B.: Hierarchical statistical modeling of xylem vulnerability to cavitation, New Phytologist, 541-554, https://doi.org/10.1111/j.1469-8137.2008.02760.x, 2009.

Paschalis, A., De Kauwe, M. G., Sabot, M., and Fatichi, S.: When do plant hydraulics matter in terrestrial biosphere modelling?, Global Change Biology, 30, e17022, https://doi.org/10.1111/gcb.17022, 2024.

Potkay, A., Trugman, A. T., Wang, Y., Venturas, M. D., Anderegg, W. R. L., Mattos, C. R. C., and Fan, Y.: Coupled whole-tree optimality and xylem hydraulics explain dynamic biomass partitioning, New Phytologist, 230, 2226-2245, https://doi.org/10.1111/nph.17242, 2021.

Powell, T. L., Wheeler, J. K., de Oliveira, A. A. R., da Costa, A. C. L., Saleska, S. R., Meir, P., and Moorcroft, P. R.: Differences in xylem and leaf hydraulic traits explain differences in drought tolerance among mature Amazon rainforest trees, Global Change Biology, 23, 4280-4293, https://doi.org/10.1111/gcb.13731, 2017.

Raghav, P., Kumar, M., and Liu, Y.: Structural Constraints in Current Stomatal Conductance Models Preclude Accurate Prediction of Evapotranspiration, Water Resources Research, 60, e2024WR037652, https://doi.org/10.1029/2024WR037652, 2024.

Restrepo-Acevedo, A. M., Guo, J. S., Kannenberg, S. A., Benson, M. C., Beverly, D., Diaz, R., Anderegg, W. R. L., Johnson, D. M., Koch, G., Konings, A. G., Lowman, L. E. L., Martínez-Vilalta, J., Poyatos, R., Schenk, H. J., Matheny, A. M., McCulloh, K. A., Nippert, J. B., Oliveira, R. S., and Novick, K.: PSInet: a new global water potential network, Tree Physiology, 44, 10.1093/treephys/tpae110, 2024.

Salomón, R. L., Limousin, J.-M., Ourcival, J.-M., Rodríguez-Calcerrada, J., and Steppe, K.: Stem hydraulic capacitance decreases with drought stress: implications for modelling tree hydraulics in the Mediterranean oak Quercus ilex, Plant, Cell & Environment, 40, 1379-1391, https://doi.org/10.1111/pce.12928, 2017.

Schenk, H. J., Espino, S., Rich-Cavazos, S. M., and Jansen, S.: From the sap's perspective: The nature of vessel surfaces in angiosperm xylem, American Journal of Botany, 105, 172–185, https://doi.org/10.1002/ajb2.1034, 2018.

Seddon, A. W. R., Macias-Fauria, M., Long, P. R., Benz, D., and Willis, K. J.: Sensitivity of global terrestrial ecosystems to climate variability, Nature, 531, 229-232, 10.1038/nature16986, 2016.

Silva, M., Matheny, A. M., Pauwels, V. R. N., Triadis, D., Missik, J. E., Bohrer, G., and Daly, E.: Tree hydrodynamic modelling of the soil–plant–atmosphere continuum using FETCH3, Geosci. Model Dev., 15, 2619-2634, 10.5194/gmd-15-2619-2022, 2022.

Sorek, Y., Greenstein, S., and Hochberg, U.: Seasonal adjustment of leaf embolism resistance and its importance for hydraulic safety in deciduous trees, Physiologia Plantarum, 174, e13785, https://doi.org/10.1111/ppl.13785, 2022.

Sperry, J. S., Donnelly, J. R., and Tyree, M. T.: A method for measuring hydraulic conductivity and embolism in xylem, Plant, Cell & Environment, 11, 35-40, https://doi.org/10.1111/j.1365-3040.1988.tb01774.x, 1988.

Sperry, J. S., Adler, F. R., Campbell, G. S., and Comstock, J. P.: Limitation of plant water use by rhizosphere and xylem conductance: results from a model, Plant, Cell & Environment, 21, 347-359, https://doi.org/10.1046/j.1365-3040.1998.00287.x, 1998.

Sperry, J. S., Hacke, U. G., Oren, R., and Comstock, J. P.: Water deficits and hydraulic limits to leaf water supply, Plant, Cell & Environment, 25, 251-263, https://doi.org/10.1046/j.0016-8025.2001.00799.x, 2002.

Steppe, K., De Pauw, D. J. W., and Lemeur, R.: Validation of a dynamic stem diameter variation model and the resulting seasonal changes in calibrated parameter values, Ecological Modelling, 218, 247-259, https://doi.org/10.1016/j.ecolmodel.2008.07.006, 2008.

Steppe, K., De Pauw, D. J. W., Lemeur, R., and Vanrolleghem, P. A.: A mathematical model linking tree sap flow dynamics to daily stem diameter fluctuations and radial stem growth, Tree Physiology, 26, 257-273, 10.1093/treephys/26.3.257, 2006.

Torres-Ruiz, J. M., Cochard, H., Delzon, S., Boivin, T., Burlett, R., Cailleret, M., Corso, D., Delmas, C. E. L., De Caceres, M., Diaz-Espejo, A., Fernández-Conradi, P., Guillemot, J., Lamarque, L. J., Limousin, J.-M., Mantova, M., Mencuccini, M., Morin, X., Pimont, F., De Dios, V. R., Ruffault, J., Trueba, S., and Martin-StPaul, N. K.: Plant hydraulics at the heart of plant, crops and ecosystem functions in the face of climate change, New Phytologist, 241, 984-999, https://doi.org/10.1111/nph.19463, 2024.

Vrugt, J. A., C.J.F. ter Braak, C.G.H. Diks, B. A. Robinson, J. M. Hyman, and D. Higdon: Accelerating Markov Chain Monte Carlo Simulation by Differential Evolution with Self-Adaptive Randomized Subspace Sampling, International Journal of Nonlinear Sciences and Numerical Simulation, 10, 273-290, doi:10.1515/IJNSNS.2009.10.3.273, 2009.

Wang, H., Guan, H., Deng, Z., and Simmons, C. T.: Optimization of canopy conductance models from concurrent measurements of sap flow and stem water potential on Drooping Sheoak in South Australia, Water Resources Research, 50, 6154-6167, https://doi.org/10.1002/2013WR014818, 2014.

Xie, S., Mo, X., Liu, S., and Hu, S.: Plant Hydraulics Improves Predictions of ET and GPP Responses to Drought, Water Resources Research, 59, e2022WR033402, https://doi.org/10.1029/2022WR033402, 2023.

Yang, J., Michaud, J., Jansen, S., Schenk, H. J., Zuo, Y. Y.: Dynamic surface tension of xylem sap lipids, Tree Physiology, 40, 433–444, https://doi.org/10.1093/treephys/tpaa006, 2020

Yang, Y., Zhang, Q., Huang, G., Peng, S., and Li, Y.: Temperature responses of photosynthesis and leaf hydraulic conductance in rice and wheat, Plant, Cell & Environment, 43, 1437-1451, https://doi.org/10.1111/pce.13743, 2020.

Zeppel, M., Macinnis-Ng, C., Palmer, A., Taylor, D., Whitley, R., Fuentes, S., Yunusa, I., Williams, M., and Eamus, D.: An analysis of the sensitivity of sap flux to soil and plant variables assessed for an Australian woodland using a soilplantatmosphere model, Functional Plant Biology, 35, 509-520, https://doi.org/10.1071/FP08114, 2008.

Zhang, Y., Lamarque, L. J., Torres-Ruiz, J. M., Schuldt, B., Karimi, Z., Li, S., Qin, D.-W., Bittencourt, P., Burlett, R., Cao, K.-F., Delzon, S., Oliveira, R., Pereira, L., and Jansen, S.: Testing the plant pneumatic method to estimate xylem embolism resistance in stems of temperate trees, Tree Physiology, 38, 1016-1025, 10.1093/treephys/tpy015, 2018.